Biochimica et Biophysica Acta 1848 (2015) 1234–1247

Contents lists available at ScienceDirect

Biochimica et Biophysica Acta

journal homepage: www.elsevier.com/locate/bbamem

Geometrical effects of phospholipid olefinic bonds on the structure and dynamics of membranes: A molecular dynamics study

Hui-Hsu Gavin Tsai *, Jian-Bin Lee, Hung-Sheng Li, Tsai-Yi Hou, Wen-Yuan Chu, Po-Chuan Shen, Ying-Yu Chen, Chun-Jui Tan, Jia-Cheng Hu, Chih-Chiang Chiu

Department of Chemistry, National Central University, Jhong-Li City, Tao-Yuan County 32001, Taiwan

ARTICLE INFO

Article history:
Received 30 November 2014
Received in revised form 3 February 2015
Accepted 13 February 2015
Available online 28 February 2015

Keywords:
Trans-phospholipid
Geometrical effect of olefinic bond
Membrane packing effect
Micro-domain

ABSTRACT

The *trans* isomers of fatty acids are found in human adipose tissue. These isomers have been linked with deleterious health effects (*e.g.*, coronary artery disease). In this study, we performed molecular dynamics simulations to investigate the structures and dynamic properties of 1-palmitoyl-2-oleoyl-*sn*-glycero-3-phosphatidylcholine (POPC) and 1-palmitoyl-2-elaidoyl *sn*-glycero-3-phosphatidylcholine (PEPC) lipid bilayers. The geometry of the olefinic bond and membrane packing effects significantly influenced the conformations and dynamics of the two C – C single bonds adjacent to the olefinic bond. For the PEPC lipid, the two C – C single bonds adjacent to the olefinic bond adopted mainly nonplanar *skew–trans* and planar *cis–trans* motifs; although the *cis* conformation featured relatively strong steric repulsion, it was stabilized through membrane packing because its planar structure is more suitable for membrane packing. Moreover, membrane packing effects stabilized the planar transition state for conformational conversion to a greater extent than they did with the nonplanar transition state, thereby affecting the dynamics of conformational conversion. The rotational motions of the first neighboring C – C single bonds were much faster than those of typical saturated C – C single bonds; in contrast, the rotational motions of the second neighboring C – C single bonds were significantly slower than those of typical saturated torsion angles. The packing of PEPC lipids is superior to that of POPC lipids, leading to a smaller area per lipid, a higher order parameter and a smaller diffusion coefficient. The distinct properties of POPC and PEPC lipids result in PEPC lipids forming microdomains within a POPC matrix.

1. Introduction

Phospholipids are the main components of cell membranes. Their structures and compositions regulate various properties of the membrane, including fluidity and permeability. Phosphatidylcholines (PCs) are the most abundant phospholipids in animal cell membranes; among them, 1-palmitoyl-2-oleoyl-*sn*-glycero-3-phosphatidylcholine (POPC) is probably the most common naturally occurring PC [1]. POPC [Fig. 1(a)] features two asymmetric acyl chains: a fully saturated *sn-1* chain and a monounsaturated *sn-2* chain with a *cis* olefinic bond. A *cis* conformation for the olefinic bond is required in lipids for their biosynthesis; it provides the stereoselective and regiospecific enzymatic activity of the desaturases [2]. The *trans* isomers of naturally occurring *cis*-unsaturated fatty acids and phospholipids have traditionally received less attention than their counterparts. With the development of advanced analytical methods, however, more new *trans*-unsaturated lipids have been identified [3], mostly in the membranes of prokaryotes and algal chloroplasts [4]. The enzymatic *trans*-to-*cis* conformational conversion of unsaturated lipids in the membranes of some bacteria is thought to be a short-term strategy for adaption under different physiologically stressful conditions. In the membranes of Gram-negative bacteria, the *trans*-to-*cis* ratio of unsaturated lipids increases in response to increased temperature [5], starvation and desiccation [6], hypo-osmotic shock [7], and the presence of organic solvents [8]. In membranes, modification in the *trans*-to-*cis* ratio of unsaturated lipids changes the membrane fluidity.

The *trans* isomers of fatty acid found in human adipose tissue are assumed to derive from dietary intake. These isomers are present in foods containing fats and oils, particularly those processed through partial hydrogenation, deodorization, or frying at high temperatures [9]. The *trans* isomers of fatty acids have also been linked to deleterious health effects (*e.g.*, coronary artery disease) and risk factors for heart attacks. The *trans* fatty acids can be incorporated into phospholipids constituting the cell membrane. Similar to the naturally occurring lipid isomers, *trans*-lipids can enter the cell metabolism process and give rise to various compounds that influence cell properties and functions [10,11].

Experimental [12,13] and molecular dynamics [14–16] studies of model membranes have revealed that the site of monounsaturation and the conformation (*cis* or *trans*) of the olefinic bond affect the order and packing of the hydrocarbon chains. The presence of *cis* olefinic bonds in lipids increases the water penetration of the model membrane

* Corresponding author. Tel.: +886 3 4227151x65909; fax: +886 3 4227664.
E-mail address: hhtsai@cc.ncu.edu.tw (H.-H.G. Tsai).

http://dx.doi.org/10.1016/j.bbamem.2015.02.016
0005-2736/

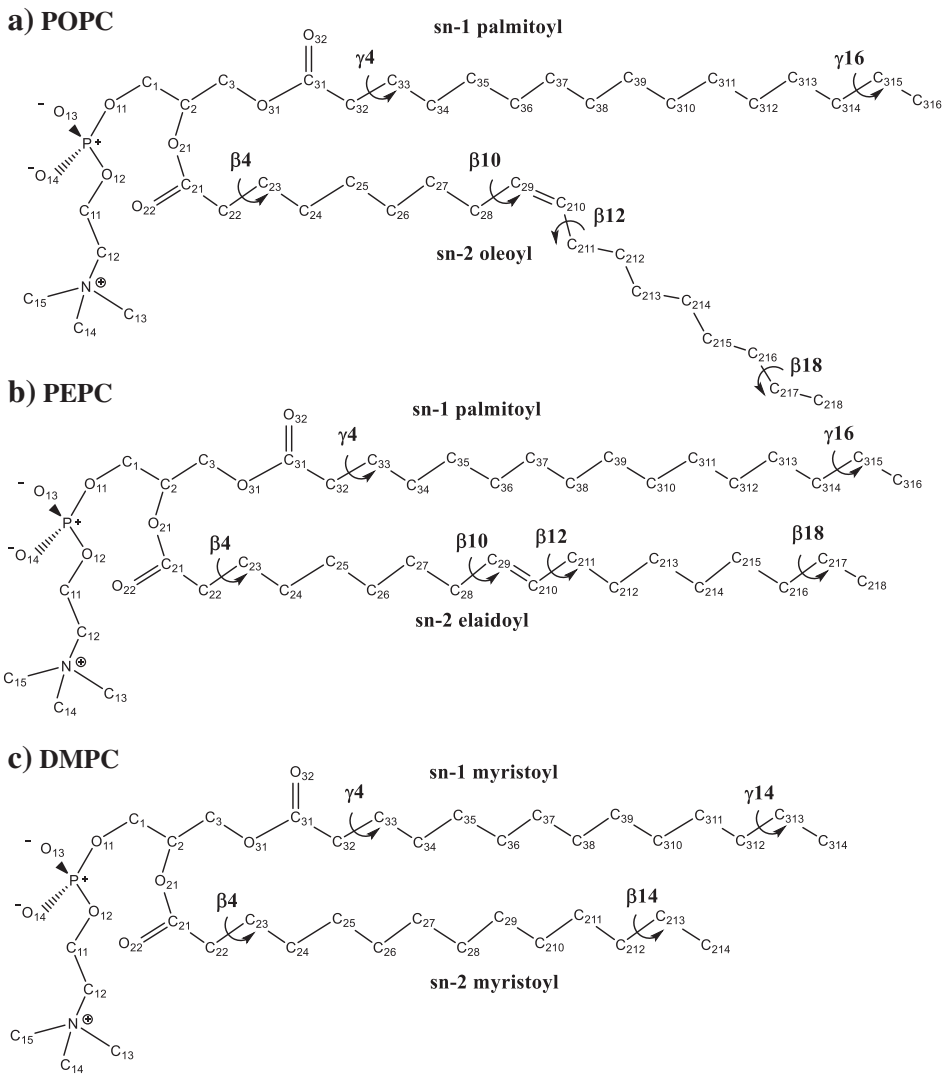

Fig. 1. The chemical structure and labeling of (a). POPC lipid, (b). PEPC lipid, and (c). DMPC lipids.

relative to that of *trans* olefinic bonds [11,17]. Moreover, the water permeability is mainly determined by the area per lipid [18]. Fluorescence measurements [17] have revealed that the fluidity of *cis* lipids is higher than that of *trans* lipids. In a mixed system of *cis* and *trans* lipids, the *trans* lipids formed ordered and thermostable domains [19].

The presence of an olefinic bond in an alkyl chain will affect the chain's conformation—in particular, the conformation of the torsion angle next to the olefinic bond. Fundamental studies of 1-butene using *ab initio* calculations [20] and microwave spectroscopy [21] have revealed that the torsion angle next to the olefinic bond adopts a *skew* or *cis* conformation. Thus, the torsion angles of single bonds next to olefinic bonds are unlikely to form the *trans* or *gauche* conformations that are usually observed in saturated alkyl chains. For mono-*cis*-unsaturated chains, X-ray diffraction experiments have indicated that the torsion angles next to the olefinic bonds prefer to populate *skew* (120°) and *skew*′ (−120°) conformations [22,23]. For better understanding, the *skew* and *skew*′ conformations of the first C–C single bond neighboring an olefinic bond present in Newman projection were displayed in the Fig. S1. Earlier short-time molecular dynamics (MD) simulations (15 ns) of POPC lipid bilayers using united-atom OPLS parameters have revealed that the torsion angles next to the *cis* olefinic bonds are broadly distributed from *gauche* (60°) to *gauche*′ (−60°) with a maximum at *trans* (180°) conformation [16]. Recent MD simulations of POPC lipid bilayers using the OPLS-AA force field [24], and of 1,2-dioleoyl-sn-glycero-3-phosphatidylcholine (DOPC) lipid bilayers [25] using a force field with olefinic bond description by Bachar et al. [26], have revealed that the torsion angles next to the *cis* olefinic bond are mainly populated at *skew* conformations; these simulation results are in good agreement with experimental observations of, for example, area per lipid and order parameters.

When considering steric effects, we might expect that the torsion angles of the single bonds next to *trans* olefinic bonds in monounsaturated lipids or fatty acids would be different from those next to *cis* olefinic bonds. The crystal structure of mono-*trans*-unsaturated elaidic acid has revealed that the torsion angles next to the *trans* olefinic bond adopt *skew* and *skew*′ conformations [27,28]. Using the united-atom force field OPLS, MD simulation [16] of 1-palmitoyl-2-elaidoyl *sn*-glycero-3-phosphatidylcholine (PEPC) in lipid bilayers has revealed that the torsion angles of single bonds next to *trans* olefinic bonds are broadly distributed in the range from −180 to +180°, peaking at the *trans* conformation. As noted in the previous paragraph, the united-atom MD simulation does not describe well the conformation of the single bonds next to the *cis* olefinic bond in POPC lipid [16]. Therefore, we suspected that united-atom MD simulations would not produce the conformations of the single bonds next to *trans* olefinic bonds, as well as other significant properties (*e.g.*, order parameters and areas per lipid), of mono-*trans*-unsaturated lipids in lipid bilayers [25]. More modern united atom force fields had been developed and had shown to well predict the structure around the cis double bond [29–31].

Table 1
System names, compositions, simulation times, and analysis times of the four studied systems.

System name	POPC	PEPC	DMPC	Total atoms	Lipid atoms	Water molecules	Na^+ ions	Cl^- ions	Times of simulation	Simulation time	Analysis time
POPC	128	–	–	30,790	17,152	4,538	12	12	3	250 ns	150- 250 ns
PEPC	–	128	–	30,790	17,152	4,538	12	12	3	250 ns	150- 250 ns
DMPC	–	–	128	28,742	15,014	4,538	12	12	3	250 ns	150- 250 ns
3O1E	96	32	–	30,790	17,152	4,538	12	12	3	350 ns	250- 350 ns

In this present study, we performed long-time-scale all-atom MD simulations using an updated force field. Our aim was to perform a systematic and comparative investigation of the geometrical effects of phospholipid olefinic bonds (*cis* or *trans*) in the *sn-2* chains of PC lipids on the structures and dynamics of their membranes. We modeled three pure lipid bilayer systems: two monounsaturated PC lipid bilayers (POPC and PEPC; mono-*trans*-unsaturated) and one fully saturated 1,2-dimyristoyl-PC (DMPC) system. To further investigate the effects of the interactions between the *cis* and *trans* olefinic bonds of the PC lipids on the structures and dynamics of the membranes, we simulated one mixed system (PEPC/POPC, 1:3). The DMPC lipid bilayers were used as a reference system. We performed relatively long MD simulations (250 ns for the pure systems; 350 ns for the mixed system) to obtain equilibrium states and better statistical results. We found that the geometries of the phospholipid olefinic bonds in POPC and PEPC and membrane packing effects significantly impacted the conformations and dynamics of the torsion angles of the first and second C – C single bonds neighboring the olefinic bonds. Membrane packing effects stabilized the planar conformations and the planar transition states (*e.g. trans*-state) of the conformational conversion of the torsion angles of the first and second C – C single bonds neighboring the olefinic bonds, thereby affecting the populations of the conformations and the dynamics of these two torsion angles.

2. Computational methods

Four lipid bilayer systems with different lipid compositions were simulated: pure POPC, pure PEPC, pure DMPC, and mixed POPC and PEPC [POPC/PEPC, 3:1 (mol/mol)]. Chemical structures and labeling of the atoms of POPC, PEPC, and DMPC are provided in Fig. 1. For convenience, the pure lipid bilayers systems are denoted herein by the abbreviation for their lipids. For example, the lipid bilayer system named "PEPC" is that containing pure PEPC. The mixed POPC/PEPC system is named "3O1E." Each lipid bilayer system comprised 128 lipids (64 for each leaflet), 4538 water molecules, 12 Na^+ ions, and 12 Cl^- ions (a salt concentration of approximately 150 mM); the corresponding water-to-lipid ratio was approximately 35. For the pure and mixed lipid systems, 250- and 350-ns MD simulations were performed, respectively and each system was performed three times with different initial configurations and velocities, yielding sufficiently converged results, with the last 100-ns trajectory used for the statistical analysis.

A web-based program, CHARMM-GUI Membrane Builder, developed by Im and co-workers [32–34] was employed to construct the initial configurations of the pure POPC lipid bilayers. The initial configuration of the mixed 3O1E system was constructed from the pure POPC system. First, 16 POPC lipids in each leaflet were chosen manually, where the shortest distance between two phosphorus atoms of these lipids was greater than 10 Å; next, the *cis*-conformation of the olefinic bonds of these chosen PEPC lipids were rotated to the *trans*-conformation (PEPC lipids) in terms of VMD software [35]. Therefore, the PEPC lipids in the mixed 3O1E system were dispersed in the POPC matrix. All MD simulations were performed with an NPT ensemble under three-dimensional periodic boundary conditions using parallel NAMD 2.7b3 [36] software. The lipids and counter ions were modeled using the CHARMM36 [37] all-atom force field; water molecules were modeled using the TIP3 model [38]. The simulation temperature was controlled at physiological temperature (310 K) in terms of Langevin dynamics. The pressure was controlled to 1 bar using the Langevin piston Nosé–Hoover method [39]; the ratio of the unit cell in the x-y plane was kept constant while allowing fluctuations along all axes. The particle-mesh Ewald technique was used to treat the long-range electrostatic interactions under the periodic boundary conditions. The bond lengths of covalent bonds with hydrogen atoms involved were constrained using the SHAKE algorithm [40], allowing the application of an integration time step of 2 fs. The cutoff distances used for pairwise interactions and for generation of the list of pairs were 12.0 and 13.5 Å, respectively. The nonbonded neighboring list was updated every 10 steps. A force switching function [41] was used to smooth the nonbonded electrostatics and van der Waals potential energy when the interatomic distance was between 9 and 12.0 Å.

Before the production simulation, energy minimization and heating simulation were performed. To remove the bad contacts of the initial configuration, energy minimization was performed first using a conjugate gradient algorithm. After 50,000 minimization steps, all simulated systems had an energy tolerance reaching 0.0001 kcal/mol. Next, a 0.3-ns heating simulation was performed in terms of Langevin dynamics [39]; a system is gradually heating to 100 K in 15 ps and is equilibrated at 100 K during a 0.1-ns simulation, and then the temperature of the system is gradually increased to 200 K in 15 ps and is equilibrated at 200 K during a 0.1-ns simulation. Finally, the system is heating to targeted temperature 310 K in 15 ps and is equilibrated at 310 K during a 0.1-ns simulation. For the production simulations, the trajectories were saved every 5 ps. Table 1 summarizes the names, compositions,

Table 2
Average area per lipid <*A*> and average thickness <*T*> of the POPC, PEPC, DMPC, and 3O1E systems.

System name	Average area per lipid (<A>, $Å^2$)			Average membrane thickness (<T>, Å)
	Total	POPC	PEPC	
POPC	65.1 ± 1.2	–	–	38.9 ± 0.6
PEPC	61.7 ± 1.3	–	–	40.6 ± 0.7
DMPC	61.0 ± 1.3	–	–	35.9 ± 0.6
3O1E	64.1 ± 1.3	64.3 ± 1.8	64.0 ± 1.4	39.3 ± 0.7
Exp. POPC	63 (297 K) [44] 62 (323 K) [46] 66 (310 K) [45]	–	–	37.0 (303 K) [49]
Exp. DMPC	60.6 (303 K) [48]			35.3 (303 K) [48]

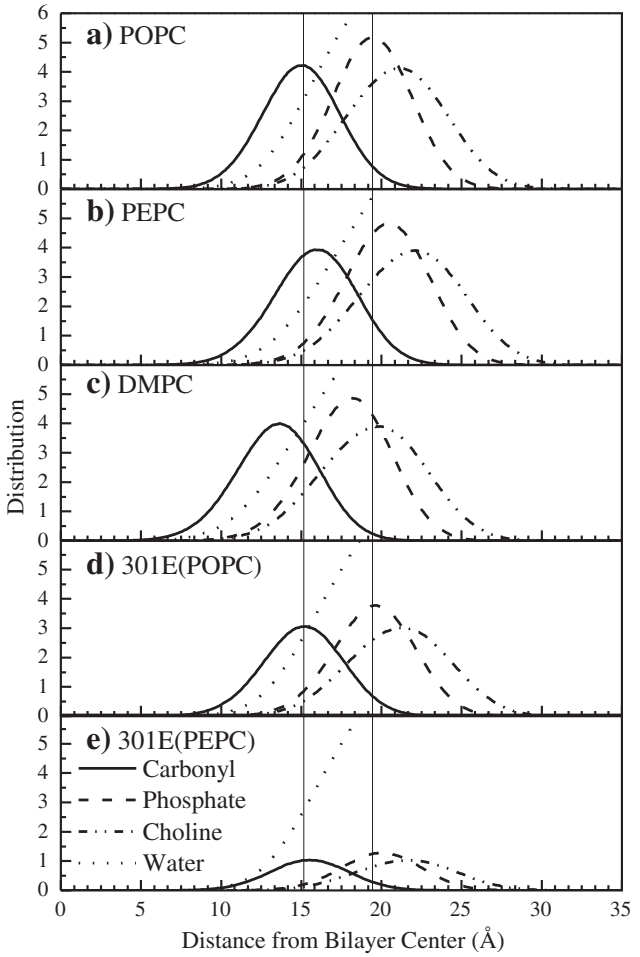

Fig. 2. Atom distributions of (a) POPC, (b) PEPC, (c) DMPC, (d) POPC lipids in 3O1E system, and (e) PEPC lipids in 3O1E system. For ready visualization and comparison, the two vertical lines are aligned at the maximum peaks of the phosphate and carbonyl groups of POPC system.

simulation times, and time intervals for the statistical analysis of each simulated system.

3. Results

3.1. Area per lipid and membrane thickness

First, we calculated the average area per lipid <*A*> and membrane thickness <*T*> of the lipid bilayers as a function of the simulation time (Fig. S2) to investigate their dependence on the lipid type and composition. Moreover, we used the values of <*A*> to determine whether the simulation systems had reached equilibrium. For the pure systems, we calculated the values of <*A*> from the lateral surface area of the simulation box divided by the number of lipids in a single leaflet. We applied a polygon-based tessellation method [42,43] with a total of 10,000 grid points (100 × 100) to calculate the value of <*A*> of a specific lipid in the mixed membrane. We calculated the values of <*T*> in terms of the shortest distance between the phosphorus atom of one lipid in a given leaflet and all of the phosphorus atoms of the lipids in the other leaflet. Thus, each lipid in one leaflet could define one membrane thickness. The values of <*T*> were averaged over the membrane thickness defined by all of the lipids in one leaflet. The values of <A> of each simulation for the POPC, PEPC, DMPC, and 3O1E systems remained stable after ca. 50 ns; For better statistical analyses, the last 100-ns equilibrium trajectories for all of the systems, having the same number of data, were used for the following statistical analyses.

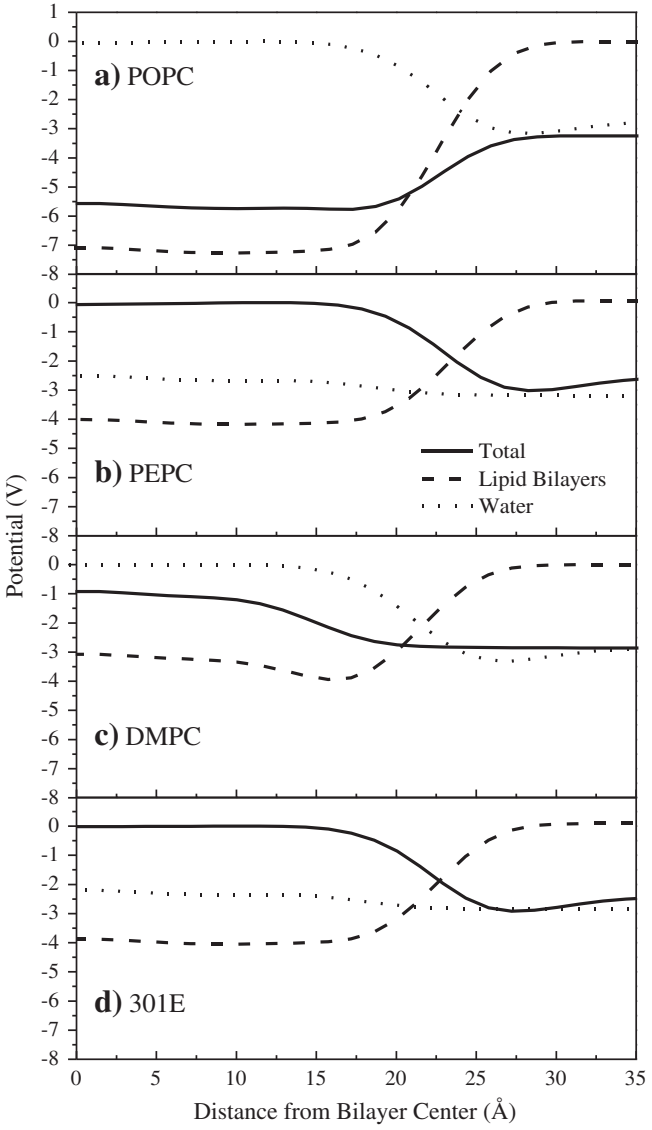

Fig. 3. The electrostatic potential profiles contributed from the lipid bilayers, water molecules, and whole system of (a) POPC, (b) PEPC, (c) DMPC, and 3O1E systems.

Table 2 lists the average values of <*A*> and <*T*> for all of our studied systems. The POPC system had the largest value of <*A*> (65.1 ± 1.2 Å^2 at 310 K), in good agreement with experimental values (63 Å^2 at 297 K [44]; 66 Å^2 at 310 K [45]; 62 Å^2 at 323 K [46]). Recently, a systematic molecular dynamics simulation study of temperature dependent bilayer structural properties has revealed that the values of <A> of PC lipid bilayers were increased with temperature [47]. Experimentally, the smaller <A> values observed at higher temperature [46] than the ones observed at lower temperature [44,45] might be due to the experimental error or different experimental conditions. On the other hand, the DMPC system had the lowest value of <*A*> (61.0 ± 1.3 Å^2), in good agreement with experimental values (60.6 Å^2 at 303 K [48]); it was 4.1 Å^2 lower than that of the POPC system. The value of <*A*> of the PEPC system (61.7 ± 1.3 Å^2) was 3.4 Å^2 lower than that of the POPC system. For the mixed system (3O1E), the overall value of <*A*> (64.1 ± 1.3 Å^2) was between those of the POPC system (upper limit) and the PEPC system (lower limit). The values of <A_{POPC}> of the POPC lipids and the values of <A_{PEPC}> of the PEPC lipids in the mixed system were different from their corresponding values in their pure systems; the value of <A_{POPC}> was less than that of the pure POPC system, while the value of <A_{PEPC}> was larger than that of the pure PEPC system. Interestingly, although the value of <A_{POPC}> was slightly larger than the value of

<A_{PEPC}>, their difference (ca. 0.3 Å^2) was much smaller than that for their corresponding pure systems (3.4 Å^2). The calculated value of <*T*> of the POPC system was 38.9 ± 0.6 Å at 310 K, in good agreement with the experimental value (37.0 Å at 303 K [49]). The calculated value of <*T*> of the DMPC system was 35.9 ± 0.6 Å at 310 K, in good agreement with the experimental value (35.3 Å at 303 K [48]). The values of <*T*> for these systems followed the order PEPC > 3O1E > POPC, opposite to that of their values of <*A*>. The good agreement between our calculated values of <*A*> and <*T*> for the POPC and DMPC systems with their corresponding experimental values support the accuracy of our simulation results.

3.2. Atom distribution

To investigate the structures of lipid bilayers, we analyzed their locations in terms of the number of atom distributions of the phosphate groups (P, O11, O12, O13, O14 atoms), choline groups (N, C12, O13, C14, and C15 atoms), carbonyl groups (C21, O22, C31, O32 atoms), and water molecules (oxygen atoms) from their corresponding lipid bilayers centers (Fig. 2). The head groups of the PEPC system protruded more toward the aqueous phase with respect to those of POPC system. These results are consistent with the calculated membrane thicknesses: the PEPC lipid bilayer was thicker than the POPC lipid bilayer. Interestingly, in the mixed 3O1E system, the atom distribution profiles of the POPC and PEPC lipids are similar with those of their corresponding pure systems.

3.3. Electrostatic potentials

The electrostatic potential determines the permeability of ionic solutes through the lipid bilayer. The electrostatic potential across the bilayer was calculated by double integration of the Poisson equation as implemented in the program GRPMACS [50],

$$\Psi(z)-\Psi(0) = -\frac{1}{\varepsilon_0}\int_0^z dz' \int_0^{z'} \rho\left(z''\right) dz'',$$

where $\rho(z)$ is the local excess charge density at point z, $\Psi(z)$ is the potential at point z, $\Psi(0)$ is the potential in the middle of the bilayer, and ε_0 is the vacuum permittivity. Fig. 3 shows the electrostatic potential profiles contributed from lipid bilayers, water molecules, and whole system of four studied systems. The electrostatic potential profiles of POPC and PEPC systems are significantly different. For the POPC system, the potential drop due to the head groups of lipids is ca. 7 V and the total potential drop in the head group region is ca. 2.5 V. However, for the PEPC system, the potential drop due to the head groups is ca. 4 V and the total potential across the head group to the membrane center is slightly increased by ca. 0.5 V, which are similar to those of DMPC system. More interestingly, the electrostatics potential profile of mixed 3O1E system is similar to that of PEPC system indicating that smaller portion (25%) of PEPC lipids could induce the electrostatic potential of mixed system similar to the pure PEPC system. Similar phenomena was also observed in the properties of lateral diffusion coefficients (*vide infra*): individual PEPC and POC lipids within 3O1E mixed system have similar lateral diffusion coefficients and are similar to that of pure PEPC system.

3.4. Order parameters of acyl chains

Fig. 4 displays the calculated order parameters and available experimental data with respect to the carbon atoms as labeled in Fig. 4. We define the deuterium order parameter of the lipid's acyl chains by the function, $S_{CD} = \frac{1}{2}\langle 3cos^2(\theta_i)-1\rangle$, where θi is the instantaneous angle between the ith segmental vector of the carbon atoms of the acyl chain and the membrane normal. The symbols < > denote the average over time and the selected ensembles.

In all cases displayed in Fig. 4, the calculated and experimental order parameters are lower than 0.25, which indicates than the aliphatic chains are disordered. For the POPC system [Fig. 4(a)], the calculated order parameters of C_{36} to C_{216} of the saturated *sn-1* chain (filled square symbols) show a continuous decrease, which are in good agreement with the experimental data (empty square symbols) [51]; simulations also reproduced the experimentally observed $|S_{CD}|$ values of C_{32} to C_{35} of the saturated *sn-1* chain, where the C_{33} has a distinctive smaller $|S_{CD}|$ value than those of its two neighboring carbons. The values of $|S_{CD}|$ for the *sn-1* chain of the POPC system were lower than those of corresponding carbon atoms of the PEPC system (filled circle symbols). On the other hand, the calculated profiles of the *sn-2* chains of POPC and PEPC lipids have a characteristic dip, due to the olefinic bond between C_{29} and C_{210} [Fig. 4(b)]. For the calculated $|S_{CD}|$ values for the unsaturated *sn-2* chains, the POPC system (filled square symbols) followed a similar trend as the experimental data (cross and empty diamond symbols) [12,52]. The values for the PEPC system (filled circle symbols) deviated considerably from the experimental data (empty circle symbols) [12]; nevertheless, the calculations and experimental data are consistent in revealing that the *sn-2* chains of the POPC system are less ordered than those of the PEPC system. More interestingly, the *cis* olefinic bond in the POPC lipid decreased the order parameters of C_{28} and C_{211} (adjacent to the olefinic bond). In contrast, the *trans* olefinic bond in the PEPC lipid did not decrease the order parameters of C_{28} and C_{211}.

For the mixed system, the calculated order parameters for the *sn-1* chains of the POPC (filled left-pointing triangle symbols) and PEPC (filled right-pointing triangle symbols) lipids were nearly identical [Fig. 4(c)] and were positioned between those of the POPC system (upper limit) and the PEPC system (lower limit) (Fig. S3). Interestingly, the order parameters of the *sn-2* chains of the POPC lipid (filled left-pointing triangle symbols) were almost identical to those in the pure POPC system (for clarity, the data are plotted together in Fig. S3). On the other hand, the *sn-2* chains of the PEPC lipids (filled right-pointing triangle symbols) were less ordered than those of the pure PEPC system (Fig. S3). These results reveal that, in the mixed system, the POPC lipids become more ordered; in contrast, the PEPC lipids become less ordered than they were in their corresponding pure system. The values of $|S_{CD}|$ of the lipids correlated with their values of <*A*>. For example, the POPC lipid provided a lower value of S_{CD} and a larger value of <*A*>.

3.5. Conformations of acyl chains

Fig. 5 presents the probability profiles for the *gauche* conformations of the four successive carbon atoms along the *sn-1* and *sn-2* chains in the POPC, PEPC, and DMPC lipids within the four studied lipid bilayers. The probability profiles of the *trans* conformations are provided in the SI (Fig. S4). We denote the C_{31}–C_{32}–C_{33}–C_{34} torsion angle in the *sn-1* chain as γ4 and label it as torsion number 4; the C_{21}–C_{22}–C_{23}–C_{24} torsion angle in the *sn-2* chain is denoted as β4 and it is labeled as torsion number 4. We define the *gauche* conformations as having torsion angles of 60 ± 30° (*gauche*, g) or −60 ± 30° (*gauche*′, g′), and *trans* conformation as having torsion angles of 180 ± 30°. The conformation profiles of the mixed lipids are very similar to those of the corresponding pure systems. Thus, we use the conformational profiles of the pure systems for our following discussion. For the *sn-1* chains [Fig. 5(a) and (c)], the probabilities of *gauche* conformations in the POPC, PEPC, DMPC lipid were almost identical except for the γ14, which DMPC lipids have a larger probability of *gauche* conformation than those of POPC and PEPC lipids. However, the probability of *gauche* conformation of the γ14 of DMPC lipids is similar to those of the γ16 of POPC and PEPC lipids. γ14 and γ16 are the last torsion angles of the *sn-1* chain of DMPC and POPC lipids, respectively.

Fig. 5(b) and (d) presents the probabilities of *gauche* conformations (zero for the β11 with the central C═C olefinic bond) of the *sn-2* chains. The presence of olefinic bonds in the POPC and PEPC lipids alters the probability of *gauche* conformations for the single bonds in the *sn-2*

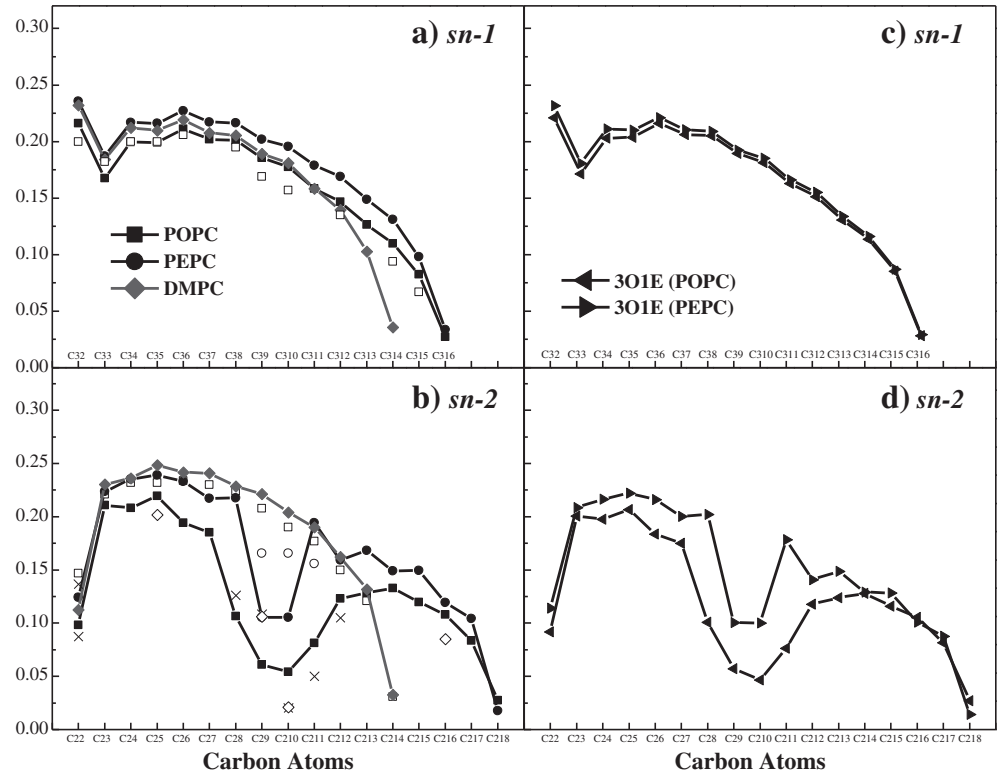

Fig. 4. Order parameters of the (a) *sn-1* and (b) *sn-2* chains in the POPC, PEPC, and DMPC systems and of the (c) *sn-1* and (d) *sn-2* acyl chains in the 3O1E system. Symbols: Experimental values of $|S_{CD}|$ for the POPC *sn-1* (□) [51] and *sn-2* (×) [12] chains at 300 K, for the POPC *sn-2* chain (◊) [52] at 303 K, for PEPC *sn-2* chain (○) [12] at 319 K, and for DMPC *sn-2* chain (□) at 303 K [63].

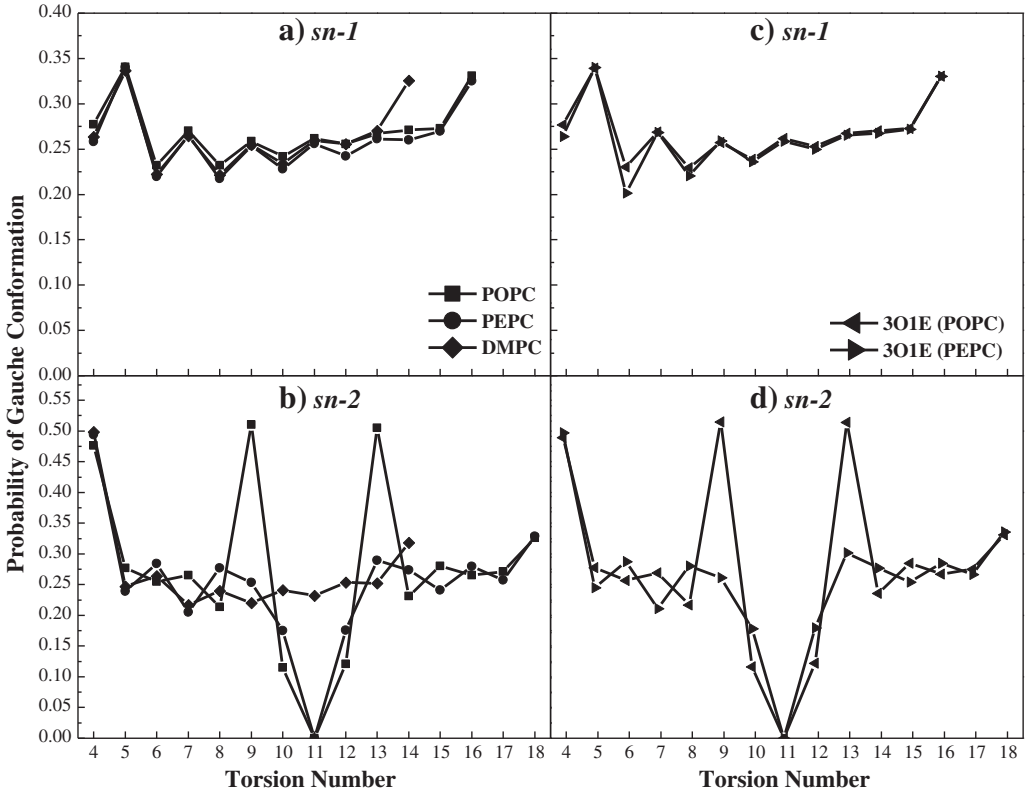

Fig. 5. Probability profiles of the *gauche* conformations of the (a) *sn-1* and (b) *sn-2* acyl chains in the POPC, PEPC, and DMPC systems and of the (c) *sn-1* and (d) *sn-2* acyl chains in the 3O1E system.

chains relative to those of their counterparts in the *sn-1* chains. The probabilities of *gauche* conformations for the β4–β8 and β14–β18 single bonds in the POPC and PEPC systems are similar indicating that the *cis*/*trans* olefinic bond geometries did not affect the conformations of these single bonds significantly. In addition, their probabilities of *gauche* conformations (except for β4 and β18) were less than 0.3; therefore, their conformations were dominated by *trans* conformations (*ca.* 0.7), which were similar to those of their corresponding saturated *sn-1* chains.

For the β10 and β12 torsion angles (first neighbors of the olefinic bonds) of the POPC and PEPC lipids, their total probabilities of *gauche* and *trans* conformations were less than 0.3. Further analysis revealed that they had other stable conformations. Fig. 6(a) displays the free energy profile of the POPC system at 310 K plotted with respect to the β10 and β12 torsion angles derived from the MD simulations. We calculated the free energy using the equation

$$\Delta G(q_1, q_2) = -k_B T \ln P(q_1, q_2),$$

where q_1 and q_2 are the β10 and β12 torsion angles, respectively, and $P(q_1,q_2)$ is a canonical probability distribution function, at temperature T, of q_1 and q_2. We observe four low energy minima located at the *skew* conformations [120 ± 30° (*skew*, *s*) or −120 ± 30° (*skew*′, *s*′)]; in particular, the (*skew*, *skew*) and (*skew*′, *skew*′) conformations of (β10, β12) in the POPC lipids are the two most stable, whereas the (*trans*, *trans*) conformation is relatively less stable. Because the *skew* conformation is not an energy minimum for a saturated alkyl chain, we performed quantum chemical calculations to further examine these results. We employed density functional theory (DFT) to calculate the rotational energy profile of a C-C single bond adjacent to a *cis* C = C double bond in the gas phase, using *cis*-oct-4-ene as the model [SI, Fig. S5(a)]. The rotational energy profile was calculated using Becke′s three-parameter exchange functional [53], the Lee–Yang–Parr gradient-corrected correlation functional [54], and the 6-31G(d,p) basis set [55], as implemented in the program Gaussian 09 [56]. The rotational energy profile was derived from the energies of full optimized geometries of *cis*-oct-4-ene except for the two fixed dihedral angles, β10′ and β12′. The DFT data revealed that the (*skew*, *skew*) and (*skew*′, *skew*′) conformations of (β10′, β12′) were the most stable, consistent with the MD simulations.

Fig. 6(b) presents the free energy profile of the PEPC system as a function of the β10 and β12 torsion angles at 310 K, derived from MD simulations. For the PEPC lipids, the β10 and β12 torsion angles are mainly populated by *cis* (0 ± 30°, *c*), *skew*, and *skew*′ conformations; the (*cis*,*cis*) basin of (β10, β12) was the most stable, by 0.7 kcal/mol relative to the second most stable basin, (*skew*′, *skew*) or (*skew*, *skew*′). Although the *cis* conformation is the most stable, the *skew* conformation was the most populated because it had two nearly degenerate energy minima, the *skew*′ and *skew* conformations; the probabilities for the *skew*, *cis*, *gauche*, and *trans* conformations of the β10 and β12 torsion angles are 0.44, 0.33, 0.18, and 0.05, respectively (Table 3). Interestingly, the *cis* conformation, the highest-energy conformation in a saturated alkyl chain, was significantly populated by the β10 and β12 torsion angles of the PEPC lipids; in contrast, the *trans* conformation of the β10 and β12 torsion angles in the PEPC lipids was relatively less stable. To further validate these results, we employed DFT at the B3LYP/6-31G(d,p) level of theory to calculate the rotational energy profile of a C – C single bond adjacent to a *trans* C═C double bond in the gas phase, using *trans*-oct-4-ene as the model molecule [SI, Fig. S5(b)]. The DFT data revealed nine energy minima, similar to those derived from MD simulations [Fig. 6(b)]. The DFT calculations predicted the (*trans*, *trans*) basin of (β10′, β12′) to be less stable than the other energy minima, consistent with the MD simulations. On the other hand, the DFT results suggested that the (*cis*, *cis*) basin of (β10′, β12′) in *trans*-oct-4-ene was less stable, by approximately 1.6 kcal/mol, than the global minimum of (*skew*, *skew*), whereas our MD simulations suggested that the (*cis*, *cis*) basin would be the most stable. Notably, our DFT calculations were performed based on the optimized geometry of a single molecule of *trans*-oct-4-ene in the gas phase, which the lipid–lipid interactions and membrane packing effect were not taken into consideration; whereas the energy profiles derived from MD simulations were calculated from simulations of 128 PEPC lipid chains within lipid bilayers at 310 K. Both the MD simulations of the PEPC lipid bilayers and the DFT calculations of *trans*-oct-4-ene validated that a single C – C bond adjacent to a *trans* olefinic bond can adopt a *cis* or *skew* conformation.

Fig. 7(a) shows the free energy profile of the POPC systems in terms of the β12 and β13 torsion angles (first and second neighbors of the olefinic bond). It reveals that the (*skew*, *trans*) basin of (β12, β13) is the most stable and that the (*skew*, *gauche*) basin is almost as stable as the (*skew*, *trans*) basin. Although the β9 and β13 torsion angles adopted mainly *gauche* and *trans* conformations, their *gauche*/*trans* ratio of 1.18 indicates that the *gauche* conformation was more populated than the *trans* conformation (Table 3).

Fig. 7(b) displays the free energy profile of the PEPC systems in terms of the β12 and β13 torsion angles, revealing that the (*cis*, *trans*) and (*skew*, *trans*) basins were the two lowest energy basins. The β9 and β13 torsion angles of the PEPC system were populated mainly by *trans* and *gauche* conformations. The *gauche*/*trans* ratios of β9 and β13

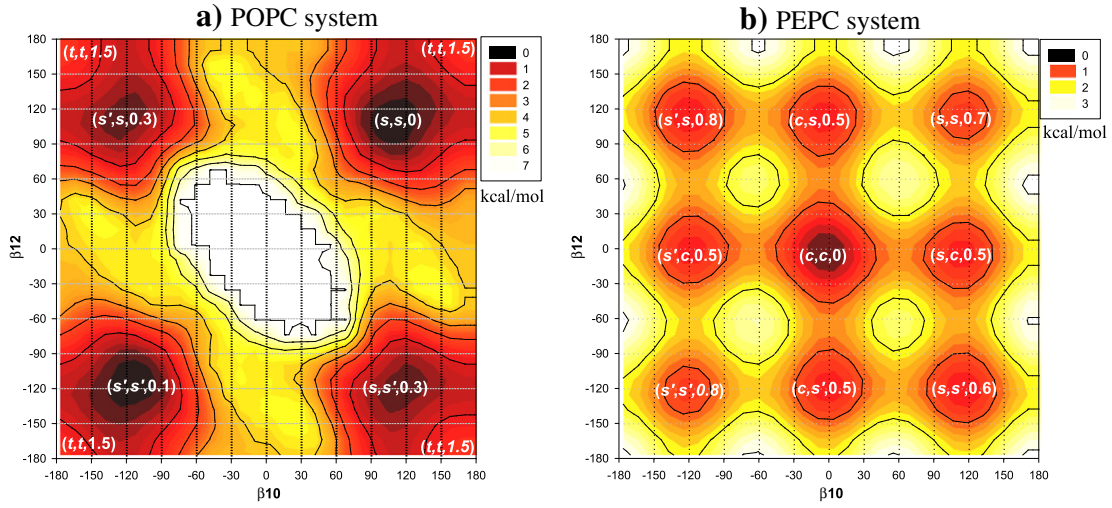

Fig. 6. Free energy profiles (in kcal/mol) of the (a) POPC and (b) PEPC systems, plotted with respect to the β10 and β12 torsion angles. The two letters and one number within the parentheses near an energy basin indicate the conformations of the β10 and β12 torsion angles and the lowest energy of the energy basin (*s*: *skew*; *s*′: *skew*′; *c*: *cis*).

Table 3
The probabilities of conformation for β9/ β13 and β10/ β12 in POPC and PEPC systems.

Torsion angle	POPC system				PEPC system			
	Trans	*Skew*	*Gauche*	*Cis*	*Trans*	*Skew*	*Gauche*	*Cis*
β10	0.17	0.71	0.12	0.00	0.05	0.44	0.18	0.33
β12	0.16	0.71	0.12	0.00	0.05	0.44	0.18	0.33
β9	0.44	0.04	0.52	0.00	0.71	0.03	0.26	0.00
β13	0.45	0.04	0.51	0.00	0.67	0.03	0.29	0.00

torsion angles were 0.37 and 0.43, respectively, similar to those of the saturated alkyl chains of the PEPC lipids (with the exception of β10 and β12). Taken together, these data suggest that the *cis* olefinic bond in the POPC lipids results in the *skew* conformation being the most stable for the adjacent C – C single bond, and increases the probability of a *gauche* conformation for the next C – C single bond along. In contrast, the *trans* olefinic bond in the PEPC lipids leads to *skew* and *cis* conformations being the most stable in the adjacent C – C single bonds.

3.6. Conformational lifetimes of the acyl chains

In the previous section we demonstrated that various torsion angles in the acyl chains of the POPC and PEPC systems formed stable conformations. This feature implies that the torsion angles in various conformations have different lifetimes and stabilities. Therefore, we calculated their lifetimes of populated conformations to determine their relative stabilities. Fig. 8 displays the lifetime profiles of the *gauche* and *trans* conformations of the acyl chains in the POPC and PEPC systems. The inset to Fig. 8 presents the lifetimes of the β10 and β12 torsion angles of the POPC lipids in their *skew* conformations and of the PEPC lipids in their *cis* and *skew* conformations. Fig. S6 provides the lifetime profiles for the *trans* and *gauche* conformations of the acyl chains in the DMPC and mixed system. For the *sn-1* chains, the corresponding torsion angles of the POPC and PEPC lipids had similar lifetimes for their *trans* and *gauche* conformations. As expected, the lifetimes of the *trans* conformations of the POPC and PEPC lipids were longer than those of their *gauche* conformations.

For the *sn-2* chains, the *trans* and *gauche* lifetime profiles of the β4–β8 and β14–β18 torsion angles of the POPC and PEPC lipids were similar, and they were also similar to their counterparts in the *sn-1* chains. The lifetimes of the *gauche* and *trans* conformations of the β9 and β13 torsion angles (second neighbors to the olefinic bonds) of the POPC and PEPC lipids were, however, longer than those of their corresponding β4–β8 and β14–β18 torsion angles. In particular, the lifetimes

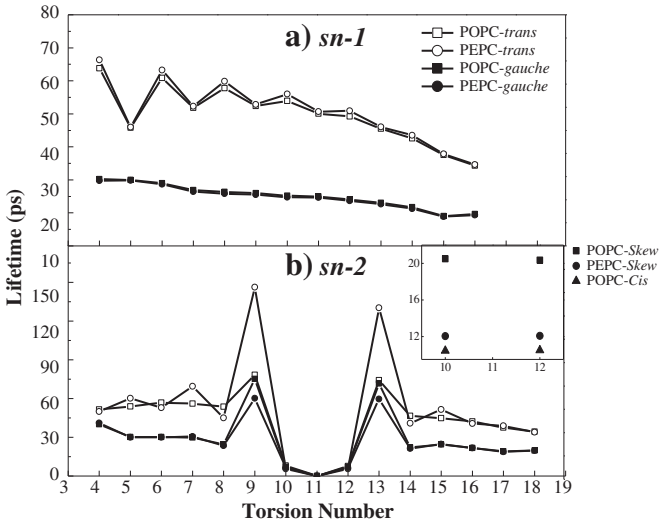

Fig. 8. Lifetime profiles of the torsion angles in the (a) *sn-1* and (b) *sn-2* alkyl chains of the POPC and PEPC systems. Inset: lifetimes of the β10 and β12 torsion angles in *skew* and *cis* conformations.

of the *trans* conformations of the β9 and β13 torsion angles in the PEPC lipids reached as high as 146 and 130 ps, respectively.

Fig. 9 displays the one-dimensional free energy profiles of the POPC and PEPC systems in terms of β13 torsion angles derived from the MD simulations. It reveals energy barriers for the *trans* to *gauche* conformational conversions of the β13 torsion angles of the POPC and PEPC lipids of 3.46 and 3.87 kcal/mol, respectively. These energy barriers are higher than those of the other single bond torsion angles in the *sn-2* chains of the POPC and PEPC lipids (*e.g.*, the energy barrier was 2.95 kcal/mol for the β15 torsion angle in the POPC lipid).

On the other hand, the lifetimes of the most-populated conformations for the β10 and β12 torsion angles of the POPC (*skew*) and PEPC (*skew* and *cis*) lipids were much shorter than those of other single bond torsion angles having *trans* conformations. The lifetimes (21.0 ps) of the most-stable *skew* conformation of the β10 and β12 torsion angles of the POPC lipids were similar to those of less-stable *gauche* conformations of other single bonds. Moreover, the lifetimes of the *cis* and *skew* conformations of the β10 and β12 torsion angles in the PEPC lipids were approximately 10.0 and 12.0 ps, respectively. Fig. 10 presents one-dimensional free energy surfaces of the POPC and PEPC

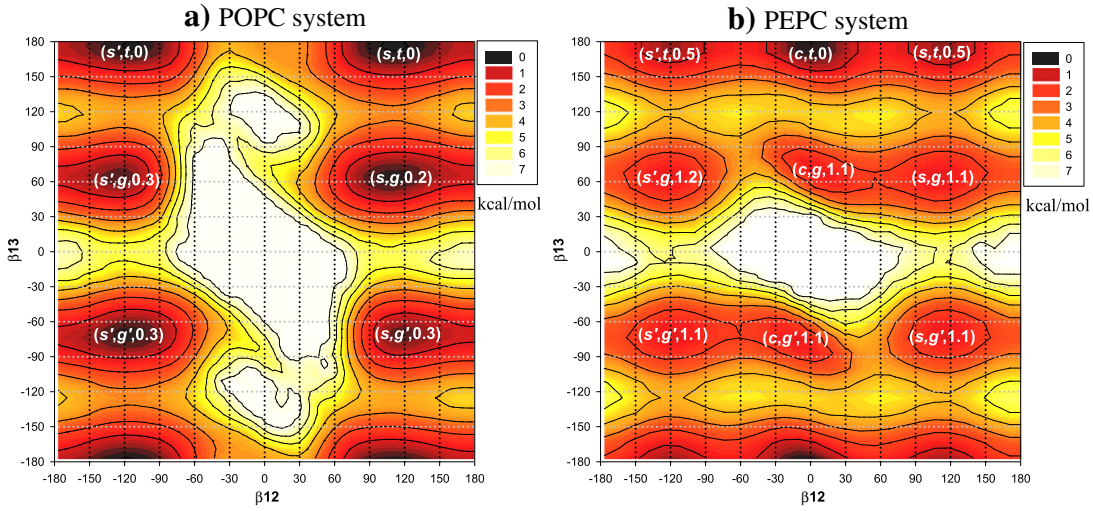

Fig. 7. Free energy profiles (in kcal/mol) of the (a) POPC and (b) PEPC systems, plotted with respect to the torsion angles β12 and β13. The two letters and one number within the parentheses nearby an energy basin represent the conformations of the β12 and β13 torsion angles and the lowest energy of the energy basin (*g*: *gauche*; *g′*: *gauche′*; *t*: *trans*; *s*: *skew*; *s′*: *skew′*; *c*: *cis*).

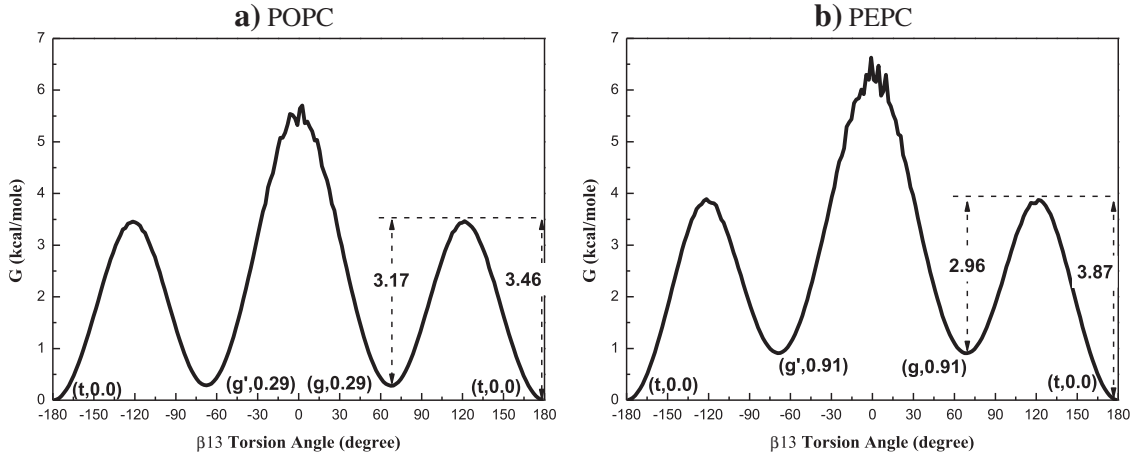

Fig. 9. One-dimensional free energy profiles (in kcal/mol) of the (a) POPC and (b) PEPC systems, plotted with respect to their β13 torsion angles. The letter and number within the parentheses near each energy basin indicate the conformation of the β13 torsion angle and the energy, respectively.

systems, plotted with respect to the β12 torsion angles derived from the MD simulations. The energy barrier for the *skew* to *skew′* conformational conversion of the β12 torsion angle in the POPC lipid was 0.73 kcal/mol; that for the *cis* to *skew* (or *skew′*) conformational conversion of the β12 torsion angle for the PEPC lipid was approximately 1.24 kcal/mol.

3.7. Dynamics of torsion angles

The chain dynamics of lipids consist primarily of dihedral angle rotations and other local motions, such as overall translation and/or rotation. A previous study revealed that the fast relaxation of alkyl chains arises mainly from isomerization [57]. In the previous section, we reported that *cis* and *trans* olefinic bonds can affect the lifetimes of their neighboring C – C single bonds, in particular their β12 and β13 torsion angles. To understand the intramolecular dynamics of the acyl chains, we calculated the dihedral angle autocorrelation function (DACF) of the β12 and β13 torsion angles of the POPC and PEPC lipids (Fig. 11). We also calculated the DACF of the β15 torsion angle of the POPC lipid for comparison. The DACF [58] is defined as

$$R_{\phi}(t) = \frac{\left(\langle \cos\phi(0)\cos\phi(t)\rangle - \left\langle \cos\phi(0)^2 \right\rangle\right)}{\left(\langle cos^2\phi(0)\rangle - \langle \cos\phi(0)^2\rangle\right)},$$

where $\phi(t)$ is the dihedral angle at time t, $\phi(0)$ is the dihedral angle at time zero, and the brackets denote ensemble averages. In Fig. 11, the relaxation times descend in the following order: β13 of PEPC lipid > β13 of POPC lipid > β15 of POPC lipid > β12 of POPC lipid > β12 of PEPC lipid. These results indicate that the dihedral angle motions of the β13 torsion angle of the PEPC lipid and the β13 torsion angle of the POPC lipid are slower than those of other single bond dihedral angles (*e.g.*, the β15 torsion angle of the POPC lipid). In contrast, the motions of the β12 torsion angle of the POPC lipid and the β12 torsion angle of the PEPC lipid were relatively fast. These DACF results are consistent with the rotational energy barriers discussed above.

3.8. Lateral diffusion coefficient

We have demonstrated that the POPC and PEPC lipids within lipid bilayers have distinct conformations and thus have different packing and fluidity. To understand the fluidity of the lipids, we calculated the lateral diffusion coefficient of the lipids in the membrane. The lateral diffusion coefficients of the lipids in the xy-directions D_{xy}, can be calculated from the mean-square-displacement as

$$D_{xy} = \frac{1}{4}\lim_{t\to\infty}\frac{<[r(t_o+t)-r(t_o)]^2>}{t},$$

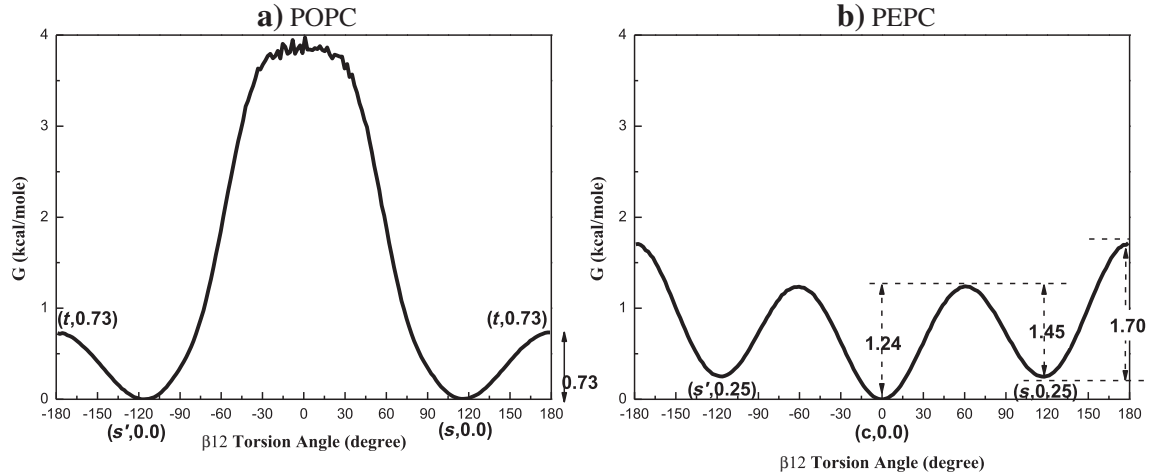

Fig. 10. One-dimensional free energy profiles (in kcal/mol) of the (a) POPC and (b) PEPC systems, plotted with respect to their β12 torsion angles. The letter and number within the parentheses nearby each energy basin indicate the conformation of the β12 torsion angle and the energy, respectively.

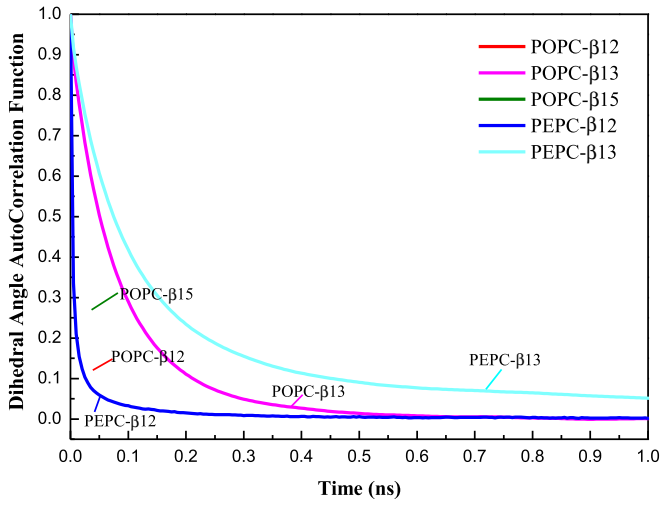

Fig. 11. DACFs of the β12, β13, and β15 torsion angles of POPC and the β12 and β13 torsion angles of PEPC.

where D_{xy} is the lateral self-diffusion coefficient, $\overrightarrow{r}(t)^2$ is the mean square displacement, and t is the elapsed time. The angled brackets < > indicate an ensemble average, which is an average over all lipids in the simulations and all origins. Fig. 12 shows the mean square displacement of lipids as a function of elapsed times (dashed lines). The solid line in Fig. 12 is the fitted results of the above equation. The D_{xy} values of the pure POPC and DMPC systems are 12.5×10^{-8} and 16.0×10^{-8} cm^2/s, respectively. which are in good agreement with their corresponding experimental values, 12.6×10^{-8} cm^2/s at 308 K [59] and 14.3×10^{-8} cm^2/s at 313 K [60]. For the pure systems, the D_{xy} value is in the order: DMPC > POPC > PEPC (9.0×10^{-8} cm^2/s). For the mixed system, the lateral diffusion coefficients of POPC (8.0×10^{-8} cm^2/s) and PEPC (8.3×10^{-8} cm^2/s) are nearly indistinguishable and are close to that of pure PEPC system.

3.9. PEPC microdomain formation in the mixed system

A previous study revealed that PEPC and PSPC can form ordered and thermostable domains [19]. In this study, we found that the POPC and PEPC lipids have different structural and dynamical properties. Thus, we suspected that they might form different domains when mixed.

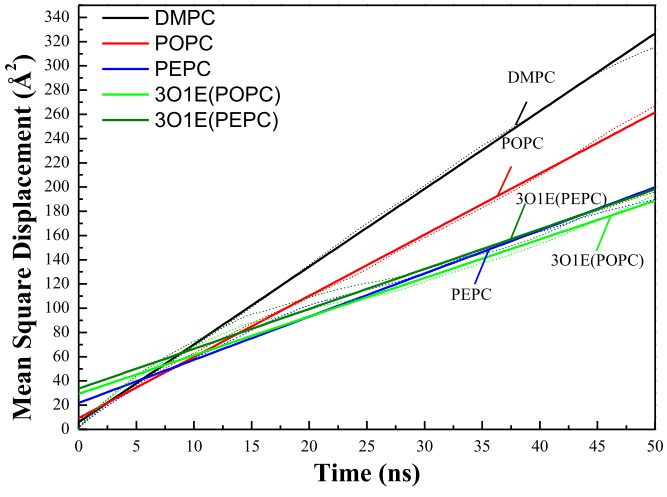

Fig. 12. The mean square displacement in the *xy* direction of the center of mass of lipids in POPC, PEPC, DMPC and 3O1E systems are shown in dashed lines. Solid lines indicate the linear fitting slopes.

Therefore, we examined whether the PEPC lipids could form microdomains within the POPC matrix. Fig. 13 displays the radial distribution functions $g(r)$ of the phosphorus–phosphorus distances of the PEPC lipids in the 3O1E mixed systems, plotted with respect to the simulation time derived from one of three simulations. The $g(r)$ of the phosphorus–phosphorus distances of other two simulations were provided in Fig. S9. The values of $g(r)$ were calculated using the equation

$$g(r) = \frac{\mathrm{N(r)}}{4\ \pi\ r^2 \rho \delta r}$$

where $N(r)$ is the number of two chosen phosphorus atoms at a distance r, δr is a spherical shell of thickness at a distance r of two chosen atoms, and ρ is the number density. The initial model of the 3O1E system was constructed with the PEPC lipids dispersed well within the POPC matrix [Fig. 14(a)]; the first peak centered near 6.5 Å has low intensity at the simulation time period of 0–50 ns. Its height increased upon increasing the simulation time to 250 ns, thereafter fluctuating during the period 250–350 ns. These results indicate that the PEPC lipids in the 3O1E system tended to aggregate during the simulation time. Table 4 lists the calculated PEPC domain sizes and their populations for the 3O1E system, with respect to the simulation time (derived from the same simulation of Fig. 13). When the distance between two phosphorus atoms of two given PEPC lipids was within 7.5 Å, we considered them to have formed one PEPC domain with size 2; similarly, we calculated other larger domains [61]. We observed that PEPG dimers were predominant during the early stages of simulation, with larger microdomains forming (*e.g.*, pentamers, hexamers), albeit with relatively lower populations, during the later stages. A snapshot at $t = 50$ ns [Fig. 14(b)] reveals sets of two and three PEPC lipids having aggregated together; a snapshot at $t = 250$ ns [Fig. 14(c)] reveals the formation of a larger PEPC lipid microdomain (comprising nine PEPC lipids); these structures were calculated using a polygon-based tessellation method [42,43]. Our simulations reveal that PEPC lipids can form microdomains within a POPC matrix.

4. Discussion

The conformations and dynamics of the acyl chains of POPC and PEPC lipids are affected by the geometry of their olefinic bonds. Within the membrane environment, the conformations and dynamics of the acyl chains of POPC and PEPC lipids can affect the packing of the membrane, and *vice versa*. MD simulations have revealed that the presence of an olefinic bond in the acyl chain of the lipid alters the conformations

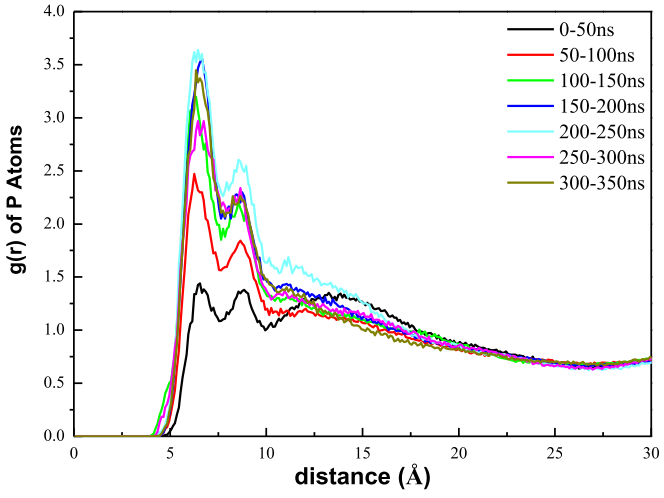

Fig. 13. Radial distribution functions $g(r)$, calculated using a 50-ns time interval, of the phosphorus–phosphorus distances between PEPC lipids in the 3O1E system.

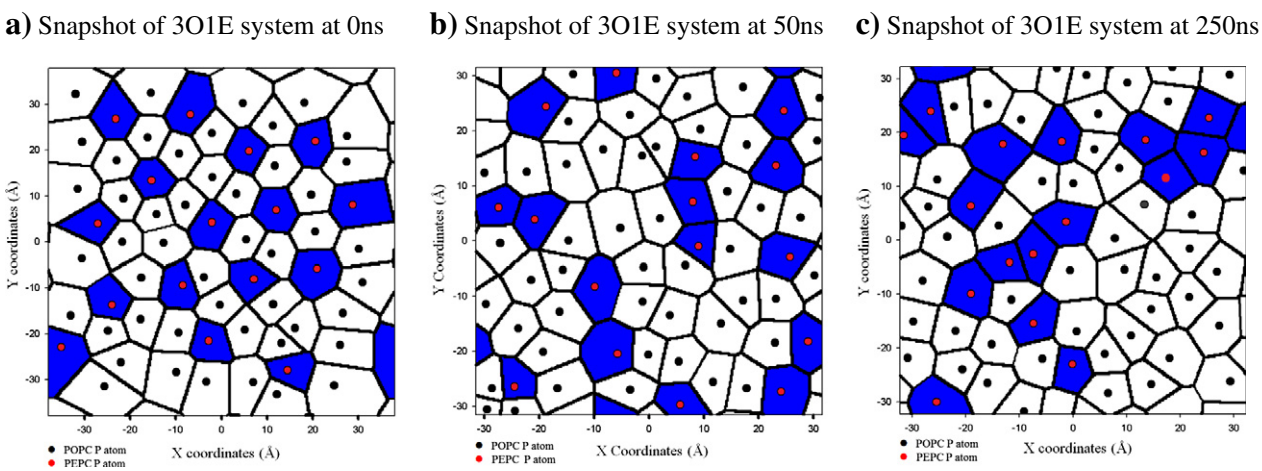

Fig. 14. Snapshots of the locations of the phosphorus atoms in the 3O1E system after simulations for (a) 0, (b) 50, and (c) 250 ns. The snapshots were calculated using a polygon-based tessellation method. The blue areas and red circles indicate the PEPC domains; and white areas and black circles indicate POPC lipids.

and dynamics of the first and second C – C single bonds neighboring the olefinic bond, with respect to those of other C – C single bonds. Previous MD simulations of POPC lipid bilayers, using a united-atom force field, revealed that the torsion angles of the saturated C – C bonds next to the *cis* olefinic bond were distributed broadly in the range between 60 and 300°, peaking at 180° (*trans*) [16]. In contrast, X-ray diffraction experiments of *cis*-monounsaturated fatty acids [22] and diacylglycerols [23] have revealed that the C – C single bonds adjacent to the *cis* olefinic bond prefer *skew* conformations. In this study, we found that in the POPC lipid, the β10 and β12 torsion angles (first neighbors to the *cis* olefinic bond) exist predominantly in *skew* conformations (*ca.* 70%), in good agreement with X-ray diffraction data [22,23]. Our MD simulations revealed that in the POPC lipid, the *trans* conformation, which commonly occurs in the saturated alkyl chains, becomes a transition state (TS) in the *skew*⇌*skew′* conversion of the β10 and β12 torsion angles. Moreover, the *gauche* conformation is not an energy minimum. Recent MD simulations of POPC lipid bilayers characterized the *skew* conformation as being the most stable conformation for the β10 and β12 torsion angle [24]. Consequently, the β10, *cis*, and β12 torsion angles of the POPC lipid form a stable *skew–cis–skew* motif, which has a nonplanar kink structure. As expected, the geometry of the *cis* olefinic bond in the POPC lipids results in the acyl chain having a kinked boomerang-like shape. Furthermore, the *skew* conformations of the β10 and β12 torsion angles of the POPC lipids result in the acyl chain adopting a twisted boomerang-like shape [62], which is less favorable for the packing of acyl chains than is a planar motif (*e.g.*, *trans–cis–trans*). Interestingly, the β9 and β13 torsion angles of POPC lipids have slightly higher *gauche* populations than they do *trans* conformations—a situation that differs from that typically found for saturated alkyl chains. This phenomenon arises because when the *cis* olefinic bond and the β10 and β12 torsion angles adopt a *cis–skew* motif, there is less repulsion between C_{213} (sp^3 carbon atom) and C_{210} (sp^2 carbon atom; more localized electron density) in the *gauche* conformations of the β9 and β13 torsion angles than there is in the saturated C – C bonds (sp^3 carbon atoms).

Microwave spectra have revealed that 1-butene exists in two rotational isomers: the *cis* and the *skew* conformations [21]. *Ab initio* calculations (MP3/6-31G*) of 1-butene have indicated that the *skew* conformation is slightly more stable than the *cis* conformation [20]. The *skew* conformation of the C – C single bond adjacent to the olefinic bond has been observed in the POPC lipid in our and other MD simulations [24]. As expected, the *cis* conformation has not been observed in the POPC lipid, due to strong steric repulsion restricted by the *cis* olefinic bond. A rare study of the crystal structure of a *trans* fatty acid has revealed that elaidic acid (*trans*-9-octadecenoic acid) has a twisted *skew* conformation of the C – C single bond next to the *trans* olefinic bond [27,28]. Our present MD simulations have revealed that the β10 and β12 torsion angles of the PEPC lipids can adopt both *skew* and *cis* conformations. Moreover, our DFT calculations of symmetric *trans*-oct-4-ene in the gas phase revealed that the *cis* and *skew* conformations of the C – C single bonds adjacent to the *trans* olefinic bond are both energy minima, further supporting the findings from our MD simulations of PEPC lipid bilayers. Previous MD simulations of PEPC lipid bilayers, using a united atom force field, suggested that the *skew* conformation of the C – C single bond adjacent to the *trans* olefinic bond was not a stable state, and that the *cis* conformation was an energy maximum [16]. Our long-timescale MD simulations, using an all-atom force field with consideration of the olefinic bond, describe well the conformations of the C – C single bonds adjacent to the olefinic bond.

The conformations of the β10 and β12 torsion angles, as well as the *trans* olefinic bond, of the PEPC lipid alter the conformations of its β9 and β13 torsion angles. Our MD simulations revealed that when the β10 and β12 torsion angles adopt *cis* conformations, the β9 and β13 torsion angles strongly favor the adoption of *trans* conformations over *gauche* conformations; these MD simulations revealed that the free energy difference between (*cis*, *trans*) and (*cis*, *gauche*) motifs for (β12, β13) in the PEPC lipids within lipid bilayers was as high as 1.1 kcal/mol—larger than the energy difference between *gauche* and *trans* conformations (*e.g.*, 0.94 kcal/mol in β15) in other saturated torsion angles. This result can be understood by considering that when the β12 and β13 torsion angles of the PEPC lipid adopt *cis* and *gauche* conformations, the *gauche* conformation of the β13 torsion angle experiences steric repulsion not only between C213 and C210 but also between C213 and C29.

A comparison of the free energy profiles of the β12 and β13 torsion angles of PEPC lipids within a membrane (Fig. 7b) and of a single PEPC lipid in vacuum (Fig. S7a) revealed that the planar *trans* conformation of the β13 torsion angle is stabilized to a greater extent than the

Table 4
Populations of PEPC domain sizes in the 3O1E system.

PEPC domain size	Time interval						
	0–50 ns	50–100 ns	100–150 ns	150–200 ns	200–250 ns	250–300 ns	300–350 ns
2	2.007	2.980	3.921	3.784	4.025	3.885	3.798
3	0.086	0.415	0.545	0.677	0.769	0.910	0.685
4	0.002	0.004	0.027	0.097	0.111	0.239	0.049
5			0.003	0.014	0.014	0.011	0.009
6			0.001	0.001	0.017	0.001	
7							

nonplanar *cis* form when the PEPC lipids are embedded within the membrane matrix. In particular, the free energy difference between the (*cis*, *trans*) and (*cis*, *gauche*) motifs of (β12, β13) for the PEPC lipid in vacuum is 0.65 kcal/mol; this value is 0.45 kcal/mol lower than the corresponding difference (1.1 kcal/mol) when the PEPC lipids are positioned within the bilayers. These results further suggest that the planar *trans–cis–trans* motif of the olefinic bond–βb12–βb13 grouping is suitable for the packing of acyl chains with enhanced van der Waals interactions. Our MD simulations revealed that the value of <*A*> of the PEPC lipid bilayer is smaller than that of the POPC lipid bilayer. Consequently, the PEPC lipids have larger order parameters for the acyl chains than those for the POPC lipids. These results for the PEPC membrane indicate that the PEPC lipids are packed more tightly in their lipid bilayers than are POPC lipids in theirs. Therefore, the *trans*, *cis*, and *trans* conformations of the olefinic bond and the β12 and β13 torsion angles, respectively, in PEPC lipids provide a coplanar motif that allows better packing of the acyl chains of the PEPC lipids within bilayers.

The presence of an olefinic bond in the acyl chain also alters the dynamics of the adjacent torsion angles. For the POPC lipid, our MD simulations revealed that the lifetimes of the *skew–skew′* conformations (the most stable) of the β10 and β12 torsion angles were significantly shorter than that of the *trans* conformation in other saturated C – C single bonds, and even shorter than those of *gauche* conformations of other saturated C – C single bonds. Consequently, the energy barrier for the *skew–skew′* conversion (0.73 kcal/mol) of the β10 and β12 torsion angles is lower than that of the corresponding *trans*-to-*gauche* conversion of other saturated C – C bonds (*ca.* 2.95 kcal/mol). These results arise because the transition state (*trans* state) of this conversion features less steric repulsion than that found in the transition state (*skew* state) of the common *trans*-to-*gauche* conversion for a saturated C – C single bond. Moreover, the MD simulation of a single POPC lipid in vacuum (Fig. S7b) revealed an activation energy of 1.06 kcal/mol for this conversion, suggesting that membrane packing stabilizes the transition state for the planar *trans* form to a greater extent than it does for the nonplanar *skew* form. These results indicate that the membrane packing enhances the rate of *skew–⇌skew′* conversion of the β10 and β12 torsion angles of the POPC lipid. We also observed membrane packing effects in the PEPC system. For the β10 and β12 torsion angles of the PEPC lipid, within the membrane, the planar *cis* form was 0.25 kcal/mol more stable than the nonplanar *skew* conformation; in vacuum, the *cis* form was only 0.08 kcal/mol more stable than the nonplanar *skew* conformation (Fig. S8a). For the β9 and β13 torsion angles of the PEPC lipid, membrane packing stabilized the planar *trans* form (Fig. S8b).

DACF analysis revealed that the rotational motions of the β10 and β12 torsion angles in POPC and PEPC lipids were faster than those of other saturated C – C bonds, due to their lower energy barriers for conformational conversion. The rotational motions of the β10 and β12 torsion angles of the PEPC lipids were broader than those of the β10 and β12 torsion angles of the POPC lipids, due to the *cis* conformational distributions of the β10 and β12 torsion angles of the PEPC lipids being highly populated, but were forbidden in the POPC lipids. On the other hand, the rotational motions of the β9 and β13 torsion angles in the POPC and PEPC lipids were slower than those of other saturated C – C bonds.

A comparison of the olefinic bond–β12–β13 torsion angles of the POPC and PEPC lipids revealed that the PEPC lipids probably formed planar *trans–cis–trans* motifs, which favored packing of the acyl chains. On the other hand, this motif for the POPC lipids was *cis–skew–trans* or *cis–skew–gauche* (*i.e.*, nonplanar). Our MD simulations revealed that the order parameters of the acyl chains in PEPC lipid bilayers were higher than those of POPC lipids. These simulations also revealed that the area per lipid of the PEPC lipid bilayers was smaller than that of the POPC lipids. This result arose because of the better packing of the PEPC lipids, due to the conformation of the *trans* olefinic bond and also the planar *cis* conformation of the first neighboring C – C single bond adjacent to the olefinic bond. Experimental investigations of PCs have revealed that *trans*-containing PCs have smaller areas per lipid, lower fluidities, and lower permeabilities than do corresponding of *cis*-containing PCs [17]. Our MD simulations have also revealed that the diffusion coefficients of PEPC lipids are smaller than those of POPC lipids. Our simulations are consistent with experimental observations.

5. Conclusion and Summary

In this study, we performed long-timescale all-atom MD simulations of POPC and PEPC lipid bilayers, as well as their mixed system, to investigate how their structural and dynamic properties are affected by the geometry of the olefinic bonds. We draw the following main conclusions:

(1) In the POPC lipid, the two C – C single bonds adjacent to the *cis* olefinic bond prefer to adopt *skew–trans* or *skew–gauche* motifs. The rotational motions of the first C – C single bonds adjacent to the *cis* olefinic bond are much faster than those of the saturated C – C bonds. On the other hand, the second C – C single bond adjacent to the *cis* olefinic bond that similar probabilities of existing in *trans* and *gauche* conformations, with rotational motions significantly slower than those of saturated C – C single bonds.
(2) In the PEPC lipid, the two C – C single bonds adjacent to the *trans* olefinic bond can adopt various conformations, including *skew–trans* and *cis–trans* motifs; the olefinic bond–β12–β13 grouping adopts a planar *trans–cis–trans* motif suitable for membrane packing; thus, it is stabilized through membrane packing. Similar to the situation for the POPC lipid, the first C – C single bond adjacent to the *trans* olefinic bond experiences fast rotational motion; this rotational motion is broader, however, than that of the corresponding C – C bonds in the POPC lipids. Again, the second C – C single bond adjacent to the *cis* olefinic bond mainly populates the *trans* conformation, and has rotational motion slower than that of typical saturated C – C bonds.
(3) Membrane packing effects stabilize the planar conformations to greater degrees than they do nonplanar conformations, affecting the conformational populations of the two C – C single bonds next to the olefinic bond. Similarly, membrane packing effects also stabilize the planar transition states of the conformational conversion to a greater extent than they do the nonplanar transition states, thereby affecting the dynamics of conformational conversion.
(4) The packing of PEPC lipid bilayers is superior to that of the POPC lipids. Thus, PEPC lipids have higher order parameters, larger areas per lipid, and smaller diffusion coefficient than do the POPC lipids. The improved packing of the alkyl chains in PEPC lipid bilayers arises not only from the conformation of the *trans* olefinic bond but also from the planar *cis* conformation of the first C – C single bond adjacent to the olefinic bond.
(5) The distinct properties of POCP and PEPC lipids lead to the PEPC lipids forming microdomains within the POPC matrix.

Our study provides new and detailed conformational and dynamic information for the two C – C single bonds adjacent to the olefinic bonds of PEPC and POPC lipids within bilayers, and provides insight into how these properties are affected by the geometries of the olefinic bonds and the effects of membrane packing.

Transparency document

The Transparency document associated with this article can be found, in the online version.

Acknowledgements

We thank the Ministry of Science and Technology of Taiwan (grant no. NSC 102-2113-M-008-008-MY2) for financial support and the National Center for High-Performance Computing and the V'ger computer cluster at the National Central University of Taiwan for allowing access to computer time and facilities.

Appendix A. Supplementary data

Chemical structures of POPC, PEPC, and DMPC lipids; average area per lipid; membrane thickness as a function of time; order parameters of pure and mixed systems; probability profiles of the *gauche* and *trans* conformations; energy profile for rotation of C – C single bonds adjacent to the C═C double bond (β10′ and β12′) of a model molecule; lifetime profiles for the *gauche* and *trans* conformations of DMPC and 3O1E systems. Supplementary data to this article can be found online at http://dx.doi.org/10.1016/j.bbamem.2015.02.016.

References

[1] N.H. Tattrie, J.R. Bennett, R. Cyr, Maximum and minimum values for lecithin classes from various biological sources, Can. J. Biochem. 46 (1968) 819–824.
[2] B.G. Fox, K.S. Lyle, C.E. Rogge, Reactions of the diiron enzyme stearoyl-acyl carrier protein desaturase, Acc. Chem. Res. 37 (2004) 421–429.
[3] C. Ferreri, C. Chatgilialoglu, Geometrical trans lipid isomers: a new target for lipidomics, Chembiochem 6 (2005) 1722–1734.
[4] M. Ohnishi, G.A. Thompson Jr., Biosynthesis of the unique trans-delta 3-hexadecenoic acid component of chloroplast phosphatidylglycerol: evidence concerning its site and mechanism of formation, Arch. Biochem. Biophys. 288 (1991) 591–599.
[5] H. Okuyama, N. Okajima, S. Sasaki, S. Higashi, N. Murata, The cis/trans isomerization of the double bond of a fatty acid as a strategy for adaptation to changes in ambient temperature in the psychrophilic bacterium, *Vibrio* sp. strain ABE-1, Biochim. Biophys. Acta 1084 (1991) 13–20.
[6] T.L. Kieft, D.B. Ringelberg, D.C. White, Changes in ester-linked phospholipid fatty acid profiles of subsurface bacteria during starvation and desiccation in a porous medium, Appl. Environ. Microbiol. 60 (1994) 3292–3299.
[7] L.J. Halverson, M.K. Firestone, Differential effects of permeating and nonpermeating solutes on the fatty acid composition of *Pseudomonas putida*, Appl. Environ. Microbiol. 66 (2000) 2414–2421.
[8] H.J. Heipieper, R. Diefenbach, H. Keweloh, Conversion of cis unsaturated fatty acids to trans, a possible mechanism for the protection of phenol-degrading *Pseudomonas putida* P8 from substrate toxicity, Appl. Environ. Microbiol. 58 (1992) 1847–1852.
[9] A. Romero, C. Cuesta, F.J. Sánchez-Muniz, Trans fatty acid production in deep fat frying of frozen foods with different oils and frying modalities, Nutr. Res. 20 (2000) 599–608.
[10] B. Woldseth, K. Retterstol, B.O. Christophersen, Monounsaturated trans fatty acids, elaidic acid and trans-vaccenic acid, metabolism and incorporation in phospholipid molecular species in hepatocytes, Scand. J. Clin. Lab. Investig. 58 (1998) 635–645.
[11] S.L. Niu, D.C. Mitchell, B.J. Litman, Trans fatty acid derived phospholipids show increased membrane cholesterol and reduced receptor activation as compared to their cis analogs, Biochemistry 44 (2005) 4458–4465.
[12] J. Seelig, N. Waespe-Sarcevic, Molecular order in cis and trans unsaturated phospholipid bilayers, Biochemistry 17 (1978) 3310–3315.
[13] S.P. Soni, J.A. Ward, S.E. Sen, S.E. Feller, S.R. Wassall, Effect of trans unsaturation on molecular organization in a phospholipid membrane, Biochemistry 48 (2009) 11097–11107.
[14] L. Janosi, A. Gorfe, Importance of the sphingosine base double-bond geometry for the structural and thermodynamic properties of sphingomyelin bilayers, Biophys. J. 99 (2010) 2957–2966.
[15] K. Murzyn, T. Rog, G. Jezierski, Y. Takaoka, M. Pasenkiewicz-Gierula, Effects of phospholipid unsaturation on the membrane/water interface: a molecular simulation study, Biophys. J. 81 (2001) 170–183.
[16] T. Rog, K. Murzyn, R. Gurbiel, Y. Takaoka, A. Kusumi, M. Pasenkiewicz-Gierula, Effects of phospholipid unsaturation on the bilayer nonpolar region: a molecular simulation study, J. Lipid Res. 45 (2004) 326–336.
[17] C. Roach, S.E. Feller, J.A. Ward, S.R. Shaikh, M. Zerouga, W. Stillwell, Comparison of cis and trans fatty acid containing phosphatidylcholines on membrane properties, Biochemistry 43 (2004) 6344–6351.
[18] J.C. Mathai, S. Tristram-Nagle, J.F. Nagle, M.L. Zeidel, Structural determinants of water permeability through the lipid membrane, J. Gen. Physiol. 131 (2008) 69–76.
[19] A. Bjorkbom, B. Ramstedt, J.P. Slotte, Phosphatidylcholine and sphingomyelin containing an elaidoyl fatty acid can form cholesterol-rich lateral domains in bilayer membranes, Biochim. Biophys. Acta 1768 (2007) 1839–1847.
[20] K.B. Wiberg, E. Martin, Barriers to rotation adjacent to double bonds, J. Am. Chem. Soc. 107 (1985) 5035–5041.
[21] S. Kondo, E. Hirota, Y. Morino, Microwave spectrum and rotational isomerism in butene-1, J. Mol. Spectrosc. 28 (1968) 471–489.
[22] F. Kaneko, J. Yano, K. Sato, Diversity in the fatty-acid conformation and chain packing of cis-unsaturated lipids, Curr. Opin. Struct. Biol. 8 (1998) 417–425.
[23] L. Di, D.M. Small, Physical behavior of the mixed chain diacylglycerol, 1-stearoyl-2-oleoyl-sn-glycerol: difficulties in chain packing produced marked polymorphism, J. Lipid Res. 34 (1993) 1611–1623.
[24] E. Plesnar, W.K. Subczynski, M. Pasenkiewicz-Gierula, Saturation with cholesterol increases vertical order and smoothes the surface of the phosphatidylcholine bilayer: a molecular simulation study, Biochim. Biophys. Acta 1818 (2012) 520–529.
[25] H. Martinez-Seara, T. Rog, M. Karttunen, R. Reigada, I. Vattulainen, Influence of cis double-bond parametrization on lipid membrane properties: how seemingly insignificant details in force-field change even qualitative trends, J. Chem. Phys. 129 (2008) 105103–105107.
[26] M. Bachar, P. Brunelle, D.P. Tieleman, A. Rauk, Molecular dynamics simulation of a polyunsaturated lipid bilayer susceptible to lipid peroxidation, J. Phys. Chem. B 108 (2004) 7170–7179.
[27] S. Ueno, T. Suetake, J. Yano, M. Suzuki, K. Sato, Structure and polymorphic transformations in elaidic acid (trans-ω9-octadecenoic acid), Chem. Phys. Lipids 72 (1994) 27–34.
[28] J.N. Low, C. Scrimgeour, P. Horton, Elaidic acid (trans-9-octadecenoic acid), Acta Crystallogr. Sect. E: Struct. Rep. Online 61 (2005) o3730–o3732.
[29] N. Bhatnagar, G. Kamath, J.J. Potoff, Biomolecular simulations with the transferable potentials for phase equilibria: extension to phospholipids, J. Phys. Chem. B 117 (2013) 9910–9921.
[30] D. Poger, A.E. Mark, On the validation of molecular dynamics simulations of saturated and cis-monounsaturated phosphatidylcholine lipid bilayers: a comparison with experiment, J. Chem. Theory Comput. 6 (2010) 325–336.
[31] S.W. Chiu, S.A. Pandit, H.L. Scott, E. Jakobsson, An improved united atom force field for simulation of mixed lipid bilayers, J. Phys. Chem. B 113 (2009) 2748–2763.
[32] S. Jo, T. Kim, V.G. Iyer, W. Im, CHARMM-GUI: a web-based graphical user interface for CHARMM, J. Comput. Chem. 29 (2008) 1859–1865.
[33] S. Jo, J.B. Lim, J.B. Klauda, W. Im, CHARMM-GUI membrane builder for mixed bilayers and its application to yeast membranes, Biophys. J. 97 (2009) 50–58.
[34] S. Jo, T. Kim, W. Im, Automated builder and database of protein/membrane complexes for molecular dynamics simulations, PLoS One 2 (2007) e880.
[35] W. Humphrey, A. Dalke, K. Schulten, VMD: visual molecular dynamics, J. Mol. Graph. 14 (1996) 33–38.
[36] L. Kale, R. Skeel, M. Bhandarkar, R. Brunner, A. Gursoy, N. Krawetz, J. Phillips, A. Shinozaki, K. Varadarajan, K. Schulten, NAMD2: greater scalability for parallel molecular dynamics, J. Comput. Phys. 151 (1999) 283–312.
[37] J.B. Klauda, R.M. Venable, J.A. Freites, J.W. O'Connor, D.J. Tobias, C. Mondragon-Ramirez, I. Vorobyov, A.D. MacKerell, R.W. Pastor, Update of the CHARMM all-atom additive force field for lipids: validation on six lipid types, J. Phys. Chem. B 114 (2010) 7830–7843.
[38] W.L. Jorgensen, J. Chandrasekhar, J.D. Madura, R.W. Impey, M.L. Klein, Comparison of simple potential functions for simulating liquid water, J. Chem. Phys. 79 (1983) 926–935.
[39] S.E. Feller, Y.H. Zhang, R.W. Pastor, B.R. Brooks, Constant-pressure molecular-dynamics simulation — the Langevin piston method, J. Chem. Phys. 103 (1995) 4613–4621.
[40] J.-P. Ryckaert, G. Ciccotti, H.J.C. Berendsen, Numerical integration of the Cartesian equations of motion of a system with constraints: molecular dynamics of n-alkanes, J. Comput. Phys. 23 (1977) 327–341.
[41] P.J. Steinbach, B.R. Brooks, New spherical-cutoff methods for long-range forces in macromolecular simulation, J. Comput. Chem. 15 (1994) 667–683.
[42] W. Shinoda, S. Okazaki, A Voronoi analysis of lipid area fluctuation in a bilayer, J. Chem. Phys. 109 (1998) 1517–1521.
[43] W.J. Allen, J.A. Lemkul, D.R. Bevan, GridMAT-MD: a grid-based membrane analysis tool for use with molecular dynamics, J. Comput. Chem. 30 (2009) 1952–1958.
[44] J.M. Smaby, M.M. Momsen, H.L. Brockman, R.E. Brown, Phosphatidylcholine acyl unsaturation modulates the decrease in interfacial elasticity induced by cholesterol, Biophys. J. 73 (1997) 1492–1505.
[45] P.A. Hyslop, B. Morel, R.D. Sauerheber, Organization and interaction of cholesterol and phosphatidylcholine in model bilayer membranes, Biochemistry 29 (1990) 1025–1038.
[46] G. Pabst, M. Rappolt, H. Amenitsch, P. Laggner, Structural information from multilamellar liposomes at full hydration: full *q*-range fitting with high quality x-ray data, Phys. Rev. E 62 (2000) 4000–4009.
[47] X. Zhuang, J.R. Makover, W. Im, J.B. Klauda, A systematic molecular dynamics simulation study of temperature dependent bilayer structural properties, Biochim. Biophys. Acta 1838 (2014) 2520–2529.
[48] N. Kučerka, Y. Liu, N. Chu, H.I. Petrache, S. Tristram-Nagle, J.F. Nagle, Structure of Fully Hydrated Fluid Phase DMPC and DLPC Lipid Bilayers Using X-Ray Scattering from Oriented Multilamellar Arrays and from Unilamellar Vesicles, Biophys. J. 88 (2005) 2626–2637.
[49] N. Kučerka, S. Tristram-Nagle, J. Nagle, Structure of fully hydrated fluid phase lipid bilayers with monounsaturated chains, J. Membr. Biol. 208 (2006) 193–202.
[50] D. van der Spoel, E. Lindahl, B. Hess, A.R. van Buuren, E. Apol, P.J. Meulenhoff, D.P. Tieleman, A.L.T.M. Sijbers, K.A. Feenstra, R. van Drunen, H.J.C. Berendsen, Gromacs User Manual Version 4.5, www.gromacs.org2010.
[51] A. Seelig, J. Seelig, Effect of a single cis double bond on the structure of a phospholipid bilayer, Biochemistry 16 (1977) 45–50.
[52] B. Perly, I.C.P. Smith, H.C. Jarrell, Effects of the replacement of a double bond by a cyclopropane ring in phosphatidylethanolamines: a deuterium NMR study of phase transitions and molecular organization, Biochemistry 24 (1985) 1055–1063.
[53] A.D. Becke, Density-functional thermochemistry. III. The role of exact exchange, J. Chem. Phys. 98 (1993) 5648.

[54] C. Lee, W. Yang, R.G. Parr, Development of the Colle–Salvetti correlation-energy formula into a functional of the electron density, Phys. Rev. B 37 (1988) 785.
[55] G.A. Petersson, M.A. Al-Laham, A complete basis set model chemistry. II. Open-shell systems and the total energies of the first-row atoms, J. Chem. Phys. 94 (1991) 6081.
[56] Gaussian 09, Revision D.01, M.J. Frisch, G.W. Trucks, H.B. Schlegel, G.E. Scuseria, M.A. Robb, J.R. Cheeseman, G. Scalmani, V. Barone, B. Mennucci, G.A. Petersson, H. Nakatsuji, M. Caricato, X. Li, H.P. Hratchian, A.F. Izmaylov, J. Bloino, G. Zheng, J.L. Sonnenberg, M. Hada, M. Ehara, K. Toyota, R. Fukuda, J. Hasegawa, M. Ishida, T. Nakajima, Y. Honda, O. Kitao, H. Nakai, T. Vreven, J.A. Montgomery Jr., J.E. Peralta, F. Ogliaro, M. Bearpark, J.J. Heyd, E. Brothers, K.N. Kudin, V.N. Staroverov, R. Kobayashi, J. Normand, K. Raghavachari, A. Rendell, J.C. Burant, S.S. Iyengar, J. Tomasi, M. Cossi, N. Rega, J.M. Millam, M. Klene, J.E. Knox, J.B. Cross, V. Bakken, C. Adamo, J. Jaramillo, R. Gomperts, R.E. Stratmann, O. Yazyev, A.J. Austin, R. Cammi, C. Pomelli, J.W. Ochterski, R.L. Martin, K. Morokuma, V.G. Zakrzewski, G.A. Voth, P. Salvador, J.J. Dannenberg, S. Dapprich, A.D. Daniels, Ö. Farkas, J.B. Foresman, J.V. Ortiz, J. Cioslowski, D.J. Fox, Gaussian, Inc., Wallingford CT, 2009.
[57] R.M. Venable, Y. Zhang, B.J. Hardy, R.W. Pastor, Molecular dynamics simulations of a lipid bilayer and of hexadecane: an investigation of membrane fluidity, Science 262 (1993) 223–226.
[58] R.H. Boyd, R.H. Gee, J. Han, Y. Jin, Conformational dynamics in bulk polyethylene — a molecular-dynamics simulation study, J. Chem. Phys. 101 (1994) 788–797.
[59] A. Filippov, G. Orädd, G. Lindblom, Influence of cholesterol and water content on phospholipid lateral diffusion in bilayers†, Langmuir 19 (2003) 6397–6400.
[60] A. Filippov, G. Oradd, G. Lindblom, The effect of cholesterol on the lateral diffusion of phospholipids in oriented bilayers, Biophys. J. 84 (2003) 3079–3086.
[61] H.H. Tsai, W.X. Lai, H.D. Lin, J.B. Lee, W.F. Juang, W.H. Tseng, Molecular dynamics simulation of cation-phospholipid clustering in phospholipid bilayers: possible role in stalk formation during membrane fusion, Biochim. Biophys. Acta 1818 (2012) 2742–2755.
[62] S. Li, H.N. Lin, Z.Q. Wang, C. Huang, Identification and characterization of kink motifs in 1-palmitoyl-2-oleoyl- phosphatidylcholines: a molecular mechanics study, Biophys. J. 66 (1994) 2005–2018.
[63] J.P. Douliez, A. Léonard, E.J. Dufourc, Restatement of order parameters in biomembranes: calculation of C – C bond order parameters from C – D quadrupolar splittings, Biophys. J. 68 (1995) 1727–1739.